university of groningen

University Medical Center Groningen

University of Groningen

Spin-lattice coupling in iron jarosite

Buurma, A. J. C.; Handayani, I. P.; Mufti, N.; Blake, G. R.; van Loosdrecht, P. H. M.; Palstra, T. T. M.

Published in:
Journal of Solid State Chemistry

DOI:
10.1016/j.jssc.2012.03.011

IMPORTANT NOTE: You are advised to consult the publisher's version (publisher's PDF) if you wish to cite from it. Please check the document version below.

Document Version
Publisher's PDF, also known as Version of record

Publication date:
2012

Link to publication in University of Groningen/UMCG research database

Citation for published version (APA):
Buurma, A. J. C., Handayani, I. P., Mufti, N., Blake, G. R., van Loosdrecht, P. H. M., & Palstra, T. T. M. (2012). Spin-lattice coupling in iron jarosite. *Journal of Solid State Chemistry*, *195*, 50-54. https://doi.org/10.1016/j.jssc.2012.03.011

Copyright
Other than for strictly personal use, it is not permitted to download or to forward/distribute the text or part of it without the consent of the author(s) and/or copyright holder(s), unless the work is under an open content license (like Creative Commons).

The publication may also be distributed here under the terms of Article 25fa of the Dutch Copyright Act, indicated by the "Taverne" license. More information can be found on the University of Groningen website: https://www.rug.nl/library/open-access/self-archiving-pure/taverne-amendment.

Take-down policy
If you believe that this document breaches copyright please contact us providing details, and we will remove access to the work immediately and investigate your claim.

Downloaded from the University of Groningen/UMCG research database (Pure): http://www.rug.nl/research/portal. For technical reasons the number of authors shown on this cover page is limited to 10 maximum.

Download date: 05-05-2023

Journal of Solid State Chemistry 195 (2012) 50–54

Contents lists available at SciVerse ScienceDirect

Journal of Solid State Chemistry

journal homepage: www.elsevier.com/locate/jssc

Spin–lattice coupling in iron jarosite

A.J.C. Buurma [a], I.P. Handayani [a], N. Mufti [b], G.R. Blake [a], P.H.M. van Loosdrecht [a], T.T.M. Palstra [a,*]

[a] Zernike Institute for Advanced Materials, University of Groningen, Nijenborgh 4, 9747 AG Groningen, The Netherlands
[b] Max Planck Institute for Chemical Physics of Solids, Nöthnitzer Str. 40, 01187 Dresden, Germany

ARTICLE INFO

Available online 16 March 2012

Keywords:
Jarosite
Phonon mode
Frustrated triangular antiferromagnet

ABSTRACT

We have studied the magnetoelectric coupling of the frustrated triangular antiferromagnet iron jarosite using Raman spectroscopy, dielectric measurements and specific heat. Temperature dependent capacitance measurements show an anomaly in the dielectric constant at T_N. Specific heat data indicate the presence of a low frequency Einstein mode at low temperature. Raman spectroscopy confirms the presence of a new mode below T_N that can be attributed to folding of the Brillouin zone. This mode shifts and sharpens below T_N. We evaluate the strength of the magnetoelectric coupling using the symmetry unrestricted biquadratic magnetoelectric terms in the free energy.

© 2012 Elsevier Inc. All rights reserved.

1. Introduction

Coupling between spins and phonons is of fundamental interest in superconductors, colossal magnetoresistive materials and magnetoelectric materials. The magnetic frustration in magnetoelectric materials with interdependent electric and magnetic degrees of freedom is considered as a key mechanism to realise coupling between the spins and lattice. A typical example is the frustrated spin spiral magnet $TbMnO_3$. In this material, magnetic interactions compete and the resulting magnetic spin-spiral structure induces a macroscopic electrical polarisation [1,2]. This can be explained with the spin current model in which a $DS_1 \times S_2$ Dzyaloshinskii–Moriya interaction, mediated by relativistic spin–orbit coupling, gives rise to antisymmetric exchange. The magnetostriction that induces the electrical polarisation in magnetoelectric spin-spiral materials is a consequence of antisymmetric exchange. The underlying spin–orbit coupling is generally weak and limits the magnetoelectric coupling strength [3].

Magnetoelectric coupling may also involve lattice striction effects, in which a polar lattice distortion is induced by magnetic order. In this case, the improper ferroelectric order and hence magnetoelectric coupling is induced by a lattice response to minimise magnetic coupling energy. It has recently been suggested that when this mechanism is at play in a triangular frustrated antiferromagnetic lattice, sizable magnetoelectric coupling might be realized [4,5]. Here, the magnetoelectric response originates entirely from spin–lattice coupling mediated by Heisenberg symmetric superexchange. In the presence of an electric field, electrostrictive effects change the metal–oxygen–metal angle which in turn affects the magnitude of the superexchange interactions (Fig. 1). Conversely, in the presence of an externally applied magnetic field, spins will start to readjust to the applied magnetic field by rotation over small angles, breaking the 3-fold rotation axis in the case of a triangular lattice. As a consequence, the lattice relaxes to accommodate the new magnetic structure, altering the metal–oxygen–metal bond angle. The ligands tend to move away from the metal–metal axis, breaking inversion symmetry and creating an electric dipole moment [6]. The ligands move while minimising the symmetric exchange coupling energy $JS_1 \cdot S_2$ with an angle-dependent J [7]. In a triangular lattice topology strong antiferromagnetic nearest-neighbour coupling and low-dimensional organisation of the magnetic structure in triangular plaquettes lead to competition between antiferromagnetic couplings from neighbouring spins known as geometrical frustration. Such a triangular structure is particularly susceptible to applied external fields. The rich phase diagram of $CuFeO_2$ [8] demonstrates that small perturbations such as externally applied fields can strongly act on the (quasi-degenerate) magnetic ground state manifold [9] to cause a drastic change in the magnetic ground state.

A typical example of a magnetically frustrated system is the jarosite family of materials $AM_3(OH)_6(SO_4)_2$. The jarosite crystal structure with space group $R\bar{3}m$ is shown in Fig. 2 and consists of layers of corner-shared octahedra (in our case $Fe(OH)_6$) capped by sheets of tetrahedra (in our case sulphate groups) that are responsible for the weak interplanar exchange coupling. The $Fe(OH)_6$ octahedra tilt to form a corrugated structure, in which the tilting angle is determined by the size of the capping group. The triangular Kagomé mesh is a geometrically frustrated antiferromagnetic system situated in the octahedral *ab* plane of the hexagonal setting of the unit cell. The Fe^{3+} ions that carry the magnetic moments reside on the vertices of the triangles

* Corresponding author. Fax: +31 50 363 4441.
E-mail address: t.t.m.palstra@rug.nl (T.T.M. Palstra).

0022-4596/$ - see front matter © 2012 Elsevier Inc. All rights reserved.
doi:10.1016/j.jssc.2012.03.011

in the Kagomé mesh and are interconnected by bridging hydroxy groups; there are four such triangles per unit cell. The magnetic structure of jarosites has been extensively studied by neutron diffraction by Townsend et al. [10], Inami et al. [11,12] and Yildirim et al. [13]. The magnetic ground state is a 120° spin-star arrangement. Subsequent layers are antiferromagnetically coupled with a propagation vector $\mathbf{k}=(0\,0\,\frac{2}{3})$. The actual spin structure is shown in the right-hand panel of Fig. 2.

If the $Fe(OH)_6$ octahedra would not tilt, then a perfect Kagomé system with a spin-liquid state that does not order at finite temperature would likely be realised [13]. The magnetic anisotropy induced by the Dzyaloshinskii–Moriya interaction causes the jarosite to order at finite temperature. Adjacent Kagomé planes are separated by layers of non-magnetic ions. The resulting separation and therefore weak interplanar exchange interaction pathways confine the magnetic interactions mostly within the plane [13]. The canted components of the magnetic moments are stacked antiparallel to give a zero net moment [14]. The magnetic space group can be inferred from Fig. 2 as $R\bar{3}m$'. This magnetic space group does not allow a linear magnetoelectric effect. However, the biquadratic magnetoelectric effect is always allowed and permits the strength of the coupling between the spins and lattice to be studied. Here we investigate this aspect of iron jarosite using a combination of Raman spectroscopy, dielectric and specific heat measurements.

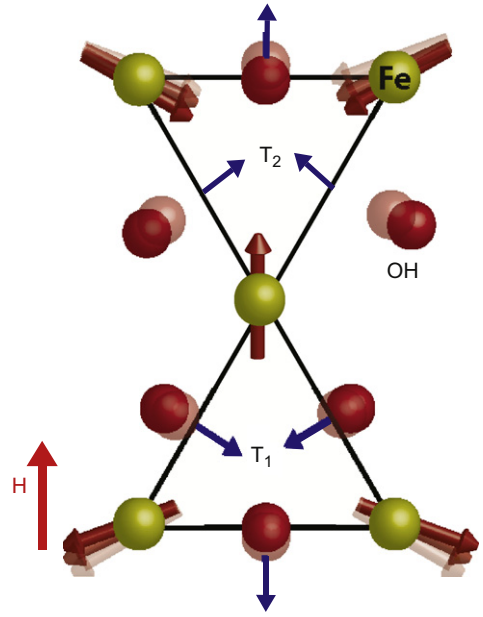

Fig. 1. Sketch of two coupled spin-triangles of KFe jarosite. The hydroxy ligands shift in such a way that the electric displacements cancel out in a pairwise fashion upon an applied magnetic field. Red vectors denote Fe^{3+} spins on the triangular apices. Ligand shifts are confined to the plane of the paper. Local dipoles that cancel out are shown in blue. (For interpretation of the references to color in this figure legend, the reader is referred to the web version of this article.)

2. Experimental

The synthesis of iron jarosite was carried out by following previous reports [15–18] under hydrothermal conditions at elevated temperature and autogenous pressure in a Parr 4745 acid digestion bomb autoclave with a 23 mL teflon beaker insert. K_2SO_4 (0.5573 g) was dissolved in 8.6 mL demi water with 0.8 g H_2SO_4 and 0.1023 g Fe wire. The mixture was heated to 488 K over 3 h, followed by a 2-h isothermal dwell before cooling down to 478 K and holding for 4 days under autogenous pressure. After four days the bomb was cooled down at −0.3 K/min. Yellow crystals of $KFe_3(OH)_6(SO_4)_2$ with triangular facets precipitated from the solution. X-ray diffraction was performed at room temperature on a crystal with dimensions $0.12\times0.10\times0.07$ mm using a Bruker APEX diffractometer operating with Mo $K\alpha$ radiation. A total of 2427 reflections were measured and the structure was refined in space group $R\bar{3}m$ to give a goodness of fit of 1.173 and a $wR(F^2)$ value of 0.0480 for 276 unique reflections. The refined lattice parameters agreed with earlier studies [12,19]: $a=7.312(3)$, $c=17.254(15)$ Å, $Z=3$. There was no evidence from the X-ray diffraction data for any lowering of symmetry from $R\bar{3}m$. Pyroelectric measurements showed that after cooling the sample to 4 K in a poling field, no pyroelectric current was measured between 4 and 300 K. This means that the sample remains centrosymmetric. Infrared spectroscopy was used to quantify the K^+ content as $0.73\le x\le1.00$ based on the intensity of the H–O–H bending mode at 1640 cm^{-1} [20]. The absent K^+ is charge compensated by H_3O^+. The H_3O^+ moiety can protonate the OH exchange bond which causes spin fluctuations. The magnetic susceptibility of the powdered sample was measured in a Quantum Design MPMS-7 magnetometer in the temperature range from 2 K to 300 K. The magnetic susceptibility data were not corrected for the gelatine container material or other diamagnetic contributions. The heat capacity at constant pressure was measured using a Quantum Design Physical Properties Measurements System (PPMS) combined with the Heat Capacity option. The sample was mounted on a platform with Apiezon grease. Dielectric measurements were performed using an Andeen Hagerling 2500A capacitance bridge; the temperature and magnetic field were controlled using the PPMS,

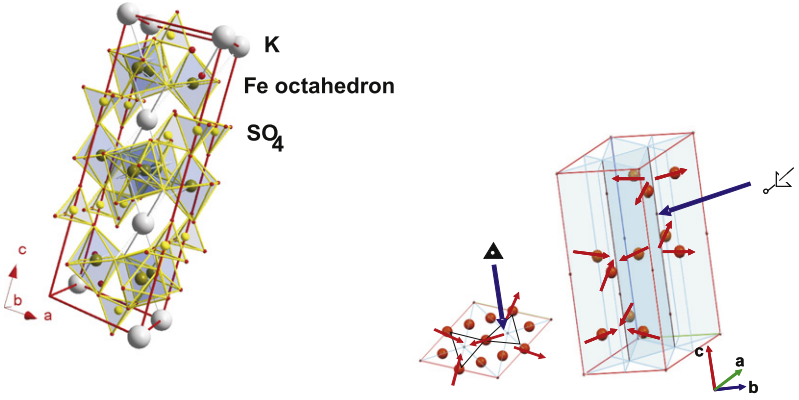

Fig. 2. (Left) Crystal structure of KFe jarosite consists of stacked layers of tetrahedral sulfate groups and layers of corner-shared $Fe(OH)_6$ octahedra. (Right) Magnetic structure of KFe jarosite adapted from Ref. [11]. The magnetic unit cell is only partially shown. The blue arrow indicates the three-fold rotoinversion axis. Mirror planes are indicated in light blue. (For interpretation of the references to color in this figure legend, the reader is referred to the web version of this article.)

which was equipped with an insert specifically wired for dielectric measurements. The capacitance and loss were recorded as a function of temperature at various constant magnetic fields. The applied voltage of the capacitance bridge was 15 V at a frequency of 1000 Hz. The single crystal sample had dimensions of slightly less than 1 mm and electrodes oriented along *a* were applied with small amounts of silver paint. The loss tangent was less than 0.01 at all temperatures. We did not align the magnetic field to a particular direction. The small size of the single crystals complicated the simultaneous orientation with respect to both the magnetic and electric fields. Polarized Raman spectra were recorded on aligned single crystals using a Jobin Yvon T64000 micro-Raman spectrometer and the 676.4 nm line of a Kr^+ laser as the excitation source. The crystals were mounted on the cold finger of an Oxford microstat (4–350 K) with a temperature stability of better than 0.1 K. The laser excitation power was kept below 50 mW/cm^2.

3. Results and discussion

3.1. Magnetic behaviour

Fig. 3 shows the magnetic susceptibility of a polycrystalline sample of $KFe_3(OH)_6(SO_4)_2$ measured in 500 Oe after cooling in zero field. Long-range order occurs at 65 K, visible as a cusp in susceptibility. A Curie–Weiss fit yields a Curie constant of 7.5 emu K (mol f.u.)$^{-1}$, corresponding to 2.52 emu K (mol Fe)$^{-1}$. The observed susceptibility differs from that reported by Grohol et al. [20] but is similar to that of Nishiyama et al. [14]. The theoretical spin-only effective moment for Fe^{3+} is 5.92 μ_B. We did not correct the susceptibility data for the temperature-independent background contribution of the gelatin capsule. Close agreement with the theoretical effective moment can be reached if the data are corrected using a temperature-independent background term of -3×10^{-3} emu (mol f.u.)$^{-1}$. We obtain a Weiss temperature of -450 K, indicating strong frustration. The above background correction shifts the Weiss temperature to -820 K, close to the previously reported value [20].

At low temperatures, a paramagnetic tail is visible due to a small fraction of uncoupled Fe spins. These unpaired spins arise from a small Fe^{3+} impurity fraction. A Curie fit of the low temperature susceptibility tail in the temperature range 10–40 K yields a Curie constant of 0.0106 emu K (mol f.u.)$^{-1}$, corresponding to a fraction of 2.8% of the spins per Fe^{3+} ion that are not ordered. It is known that the iron lattice occupancy and magnetic ordering temperature are intimately related. We therefore checked the magnetic susceptibility of single crystals mounted on a glass fibre, which showed identical properties to the polycrystalline sample.

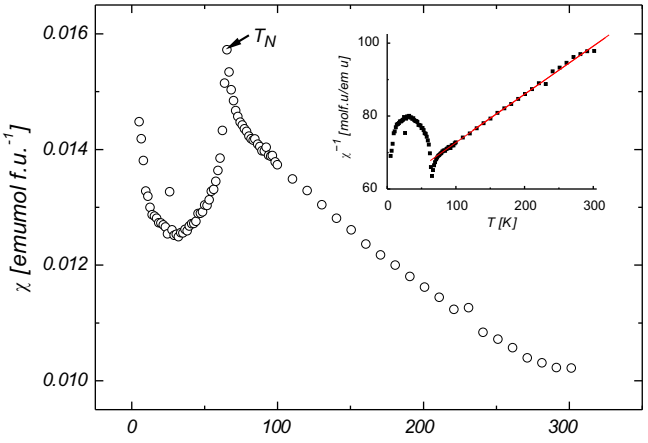

Fig. 3. Magnetic susceptibility versus temperature for polycrystalline KFe jarosite, measured on warming in 500 Oe after zero-field-cooling, showing distinct magnetic ordering at 65 K. The inset shows a Curie–Weiss fit to the inverse susceptibility in the high-temperature region.

3.2. Specific heat

The low temperature specific heat of iron jarosite is shown in Fig. 4. We observe a lambda anomaly, corresponding to the antiferromagnetic ordering at 65 K. No anomalies corresponding to volume changes other than thermal expansion or to further phase transitions were observed below the Néel temperature. The 65 K anomaly is likely a transition of purely magnetic origin.

To develop a qualitative idea of the relevant energy scales, we have analysed the lattice contribution of the specific heat, following the approach of Ramirez et al. [21]. The lattice contribution can be described in terms of Einstein and Debye phonon contributions. Plotting C/T^3 against ln T yields a graph in which the Debye and Einstein contributions can easily be distinguished. The employed model only treats the data in a phenomenological way and does not provide information on the vibrational degrees of freedom in our system. We could fit the heat capacity with two optical Einstein modes of 15 meV and 9.2 meV, and a Debye contribution with $k_BT_D=25.8$ meV. This qualitative analysis of the heat capacity shows that a low energy lattice mode is present.

The low-temperature upturn in Fig. 4 is caused by a linear temperature dependent term in the specific heat, which is typically caused by defects or impurity states. This low-temperature upturn, which was also observed by Mazjlan et al. [22], is not taken into account in our phenomenological model.

3.3. Raman spectroscopy

The Raman spectra, with the incoming and scattered light polarized along the crystallographic *b*-axis, are in good agreement with spectra previously reported [23] except for a double peaked scattering band observed near 52 cm^{-1} at low temperatures. As Fig. 5a shows, this band appears just below the magnetic ordering transition as a weak, broad feature that sharpens up and shifts to higher energy upon further lowering the temperature. The intensity of this band follows the order parameter of the magnetic structure [12], as shown in Fig. 5b which displays the zeroth moment of the spectra as a function of temperature. Above 30 K, the line can be fitted well with one Lorentzian. Near 30 K the

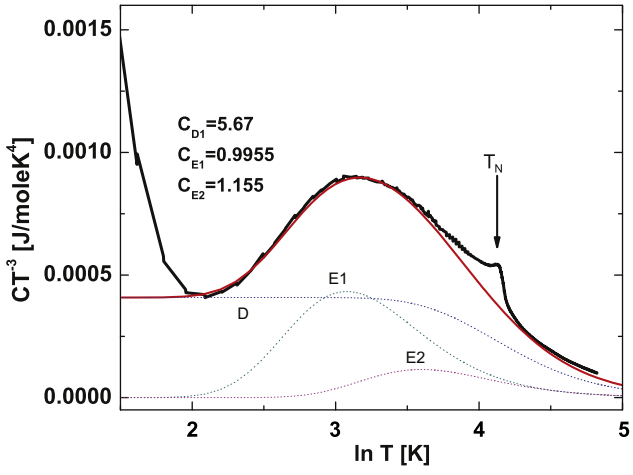

Fig. 4. Specific heat of KFe jarosite fitted with one Debye mode ($T_D=300$ K) and two Einstein modes, $T_{E1}=107$ K (74.3 cm^{-1}) and $T_{E2}=175$ K (121.5 cm^{-1}). The summed contribution is indicated in red. The magnetic ordering is clearly observable at T_N. (For interpretation of the references to color in this figure legend, the reader is referred to the web version of this article.)

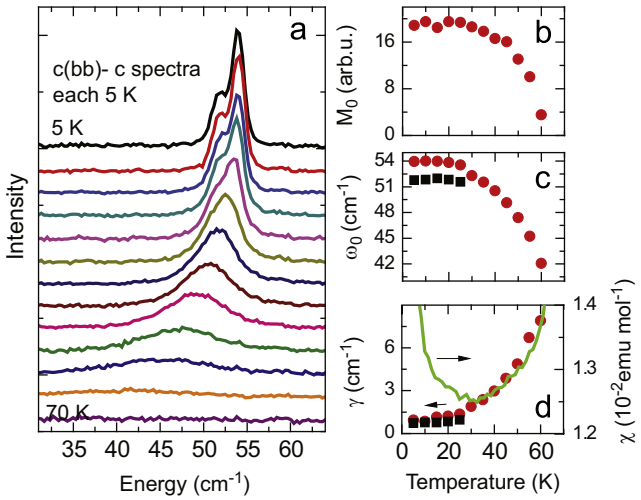

Fig. 5. Low energy (bb) polarised Raman spectra showing a new scattering band below T_N. (a) Temperature evolution of spectra between 5 and 70 K at intervals of 5 K. The spectra have been normalised to the integrated intensity of the strong phonon centred at 240 cm^{-1} and have been given an incremental offset for clarity. (b) Temperature dependence of the zeroth moment M_0 (integrated from 20 to 70 cm^{-1}). (c) Temperature dependence of the energy of the observed modes obtained from Lorentzian fits to the data (red circles are 54 cm^{-1} mode, black squares are 52 cm^{-1} mode). (d) Temperature dependence of the line-width of the observed modes (red circles are 54 cm^{-1} mode, black squares are 52 cm^{-1} mode) obtained from Lorentzian fits to the data. The magnetic susceptibility (green line) is superimposed. (For interpretation of the references to color in this figure legend, the reader is referred to the web version of this article.)

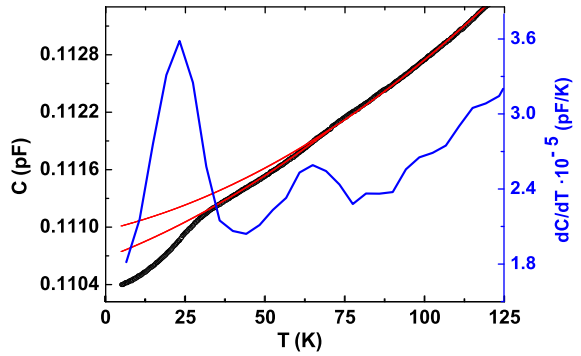

Fig. 6. Temperature dependence of the capacitance measured with electric field $E \parallel a$-axis. Extrapolations of the lattice contribution to the capacitance (red lines) show deviations below 65 K and 30 K. The derivative of the capacitance with respect to temperature (blue line) reveals two peaks at 65 K and 25 K. (For interpretation of the references to color in this figure legend, the reader is referred to the web version of this article.)

mode starts to show a low-energy shoulder that evolves into a clear double peak structure at lower temperatures. The frequencies of the observed modes, obtained by fitting Lorentzian functions to the data, are shown in Fig. 5c. The energy of the band is quite close to that of the $k=0$ magnon excitation observed in inelastic neutron scattering [24], suggesting that the origin of the 52 cm^{-1} double peak feature observed here could be due to a single magnon scattering process. However, magnetic field dependent experiments (up to 0.5 T) did not show any field-induced energy shift of the band. We therefore assign the observed band to phonon scattering, which is activated below T_N due to a magneto-elastic distortion of the crystal structure. Analysis of the second moment of the spectra shows that the splitting of the band occurs at 30 K, the temperature at which the largest anomaly in the static dielectric response is observed. It is presently not clear whether this splitting is caused by a further magneto-elastic distortion, or by a change in the coupling of the phonon to the nearby magnon excitation due to for instance a spin-reorientation transition. That the phonon couples strongly to the magnon excitations is demonstrated in Fig. 5d, which shows a strong correlation between the phonon line widths and the magnetic susceptibility, both diverging near T_N and suggesting that the most important decay mechanism for the phonon is phonon–magnon scattering.

3.4. Dielectric behaviour

The dielectric measurements are shown in Fig. 6. The derivative of the capacitance with respect to temperature shows two peaks. A weak dielectric anomaly was observed at the antiferromagnetic ordering temperature of 65 K. This weak anomaly becomes apparent after the quadratic extrapolation of thermal expansion effects, shown as the upper red line in Fig. 6. A second, stronger anomaly occurs at 25 K. This can be attributed to a weak biquadratic higher-order magnetoelectric coupling as observed earlier in materials such as $BaMnF_4$ [25].

Spin–lattice coupling is the microscopic mechanism responsible for magnetoelectric coupling here. Although this weak coupling could originate from relativistic effects, we restrict our discussion to displacements originating from exchange striction. In the KFe jarosite structure, a dipole compensation mechanism described below leaves the barycenter of charges intact by symmetry. Therefore, the observation of a magnetic-field induced net electric polarisation is symmetry prohibited. However, the polarisability does change and within the Kagomé plane, a dipole compensation mechanism occurs that relies on exchange striction. Fig. 1 shows a basic unit of the Kagomé plane, which consists of two triangular units of Fe ions T_1 and T_2 that are connected by their apices. Within a single layer, the sign of the linear magnetoelectric contributions of adjacent T_1 (up) and T_2 (down) triangles to the net magnetoelectric coupling α_{ij} cancel out (see Fig. 1). The net polarisation induced by the local dipole moments of T_2 cancels against the net polarisation generated by the local dipole moments of triangle T_1. Although there is finite spin–lattice coupling, the ligand shifts are in opposite directions and the corresponding dipole moments cancel out exactly. As a consequence, no bulk magnetically induced electric polarisation is observed due to this compensation mechanism. This agrees with the fact that a linear magnetoelectric effect is symmetry forbidden for the magnetic space group $R\bar{3}m$'. However, we should be able to observe higher-order magnetoelectric coupling terms irrespective of whether such a dipole compensation mechanism actually occurs. The biquadratic magnetoelectric coupling term δE^2H^2 is often reflected in the behaviour of the dielectric constant ϵ with magnetic field and temperature and is always symmetry allowed. We will therefore discuss the effect of magnetic field and temperature on the dielectric properties of iron jarosite and focus on the term δE^2H^2 which gives rise to an anomaly in the dielectric constant proportional to the invariant P^2L^2 and to a magnetocapacitance effect described by P^2H^2. Here, L is the antiferromagnetic order parameter. The P^2H^2 term gives a quadratic increase in the dielectric constant with magnetic field. The capacitance measured at 0 T is almost identical to that measured in a field of 8 T. Magnetocapacitance is therefore exceedingly small in our measurements. The temperature dependence of the dielectric constant ϵ as well as the shift of the low-wavenumber Raman mode with temperature suggest the presence of the term P^2L^2, where the antiferromagnetic order parameter L^2 depends on temperature. Typically this term, being unrestricted by symmetry considerations, causes a slight decrease in dielectric constant due to (in the free energy) phonon hardening via the Lyddane–Sachs–Teller mechanism [26].

The P^2L^2 term manifests itself as an anomaly in the $\epsilon(T)$ curve at T_N upon the emergence of antiferromagnetic order, as the antiferromagnetic order parameter L^2 depends on temperature. Fig. 6 shows quadratic extrapolations of the measured higher temperature $\epsilon(T)$ curve below the two dielectric anomalies. Two mechanisms are responsible for the decrease in dielectric constant if it is related to magnetic ordering: magnetostriction and spin–phonon coupling [26]. Contractive magnetostrictive effects in antiferromagnets are known to increase phonon energies (phonon hardening) and hence cause a Lyddane–Sachs–Teller related decrease of the dielectric constant. Our low temperature X-ray powder diffraction measurements indicated that the dielectric anomalies are not accompanied by a sudden change in lattice parameters. Another possible mechanism is a change in spin–magnon coupling. This coupling increases the energy of the low lying optical polar phonon, which lowers the dielectric constant.

The dielectric anomaly at 30 K is not reflected clearly in the specific heat data. However, we do observe an anomaly in capacitance at 30 K and a shoulder on the low-lying Raman mode below 35 K. Low temperature X-ray powder diffraction did not show any signs of a structural transition. Therefore, this feature probably corresponds to a second magnetic transition. Previous neutron scattering studies on jarosites do not report a magnetic phase transition below 65 K. However, it is well known that magnetic phase transitions in frustrated systems like $YMnO_3$ may escape detection in neutron scattering because different magnetic structures do not necessarily yield unique neutron diffraction patterns [27].

4. Conclusions

We observe no linear magnetoelectric coupling in iron jarosite, in agreement with the magnetic space group. However, this does not rule out higher-order magnetoelectric coupling terms. This coupling can originate from a superexchange-induced mechanism. We have employed magneto-dielectric measurements to study the symmetry unrestricted biquadratic magnetoelectric coupling terms between spin and lattice. We indeed observe a small biquadratic magnetoelectric coupling below T_N. The observation of a low-lying optical mode in Raman spectroscopy below the Néel temperature is evidence for spin–phonon coupling. The exact nature of the excitation is unclear and can be a phonon mode, an electromagnon or bimagnon. The shift in this Raman-active mode with temperature provides evidence for spin–lattice coupling. Below T_N this optical mode hardens with a concomitant change in peak width. Spin–lattice coupling is responsible for the observed biquadratic magnetoelectric effect. The effect is not large and a shift of 5 cm^{-1} corresponds to change of 1% in the dielectric constant. This is a result of the structural rigidity of the triangular lattice that is reinforced by the sulfate tetrahedra that tether the apices of the octahedra. Low temperature specific heat and X-ray diffraction experiments show that apart from magnetic ordering, no further structural phase transitions take place below 65 K.

Acknowledgments

F. De Haan and J. Baas are gratefully acknowledged for their technical support. The authors are indebted to U. Adem and B. Noheda for in-depth discussions, and thank A. Caretta for Raman measurements in magnetic field.

References

[1] T. Kimura, Annu. Rev. Mater. Res. 37 (2007) 387–413.
[2] N. Mufti, A.A. Nugroho, G.R. Blake, T.T.M. Palstra, Phys. Rev. B 78 (2008) 024109.
[3] T. Moriya, Phys. Rev. 120 (1960) 91–98.
[4] N. Spaldin, M. Mostovoy, K.T. Delaney, Phys. Rev. Lett. 102 (2009) 157203.
[5] G.A. Gehring, Ferroelectrics 161 (1994) 275–285.
[6] N.A. Spaldin, M. Mostovoy, M. Fiebig, J. Phys.: Condens. Mater. 20 (2008) 434203.
[7] K. Yamauchi, S. Picozzi, J. Phys.: Condens. Mater. 21 (2009) 064203.
[8] T.T.A. Lummen, C. Strohm, H. Rakoto, P.H.M. van Loosdrecht, Phys. Rev. B 81 (2010) 224420.
[9] R. Ballou, B. Canals, M. Elhajal, C. Lacroix, A.S. Wills, J. Magn. Magn. Mater. 262 (2003) 465–471.
[10] M.G. Townsend, G. Longworth, E. Roudaut, Phys. Rev. B 33 (1986) 4919–4926.
[11] T. Inami, S. Maegawa, M. Takano, J. Magn. Magn. Mater. 177 (1998) 752–753.
[12] T. Inami, M. Nishiyama, S. Maegawa, Y. Oka, Phys. Rev. B 61 (2000) 12181–12186.
[13] T. Yildirim, A.B. Harris, Phys. Rev. B 73 (2006) 214446.
[14] M. Nishiyama, T. Morimoto, S. Maegawa, T. Inami, Y. Oka, Can. J. Phys. 79 (2001) 1511–1516.
[15] D.G. Nocera, B.M. Bartlett, D. Grohol, D. Papoutsakis, M.P. Shores, Chem. Eur. J. 10 (2004) 3850–3859.
[16] D. Grohol, D.G. Nocera, J. Am. Chem. Soc. 124 (2002) 2640–2646.
[17] A.S. Wills, A. Harrison, C. Ritter, R.I. Smith, Phys. Rev. B 61 (2000) 6156–6169.
[18] A. Martin, A. Feltz, Z. Anorg. Allg. Chem. 575 (2004) 115–120.
[19] T. Kato, Y. Miúra, Mineral. J. 8 (1975) 419–430.
[20] D. Grohol, D.G. Nocera, D. Papoutsakis, Phys. Rev. B. 67 (2003) 064401.
[21] A.P. Ramirez, G.R. Kowach, Phys. Rev. Lett. 80 (1998) 4903–4906.
[22] A.P. Ramirez, G.R. Kowach, Phys. Chem. Mineral. 37 (2010) 635–651.
[23] C.H. Chio, S.K. Sharma, L.-C. Ming, D.W. Muenow, Spectrochim. Acta A 75 (2010) 162–171.
[24] K. Matan, D. Grohol, D.C. Nocera, Y. Yildirim, A.B. Harris, S.H. Lee, S.E. Nagler, Y.S. Lee, Phys. Rev. Lett. 96 (2006) 247201.
[25] D.L. Fox, D.R. Tilley, J.F. Scott, H.J. Guggenheim, Phys. Rev. B 21 (1980) 2926–2936.
[26] G.A. Samara, J.F. Scott, Solid State Commun. 21 (1977) 167–170.
[27] M. Fiebig, V.V. Eremenko, I.E. Chupis, Magnetoelectric interaction phenomena in crystals, MEIPIC-5 (Sudak, Ukraine, 21–24 September 2003), Kluwer, Dordrecht, 2004, p. 116.